Chapter 4
High-Performance Surface Grinding

J.C. Aurich, A. Bouabid, P. Steinmann, and B. Kirsch

Abstract. This chapter presents experimental as well as modelling and simulation approaches to investigate a high-performance surface grinding process. The complex material removal mechanisms generate transient cutting forces that cover a wide range of excitation frequencies. The generated cutting forces impact the grinding machine and lead to deformations, which depend on the machine's mechanical properties. In general, these deformations have an influence on the cutting forces. Deformations lead to a change of the depth of cut and, therefore, the cutting forces change. Thus, there are three aspects of great importance: the process, the machine and the process machine interaction. Advances in investigating the process are covered first. Afterwards, a new approach to model the machine, its deformation behavior and the way the machine interacts with the process will be described.

4.1 Introduction

In contrast to machining processes with defined cutting edges, grinding is affected by a large number of cutting edges. These cutting edges are single grains, whose number, geometry and relative position to the workpiece are not known. Although the depth of cut in high-performance surface grinding is in the range of millimeters, the depth of cut of the single grains is in the sub-micrometer range. For this reason, process machine interactions (PMI) in the range of micrometers have great influence on the single grains and hence on the complete process [1; 2; 3].

To approximate these PMI, a process model was coupled with a machine model. The process model, a kinematic-geometrical simulation of surface grinding (KSIM), is able to deliver undeformed chip parameters of each single grain in the contact zone and a high-frequency signal of the grinding force for each point of the time discretization. Based on the simulated grinding force, the machine model, a finite element model for spinning motions (SFEM), simulates PMI of the modeled machine structure in terms of the resulting displacements of the grinding wheel.

Experimental and numerical studies will be presented. The experimental investigations have been carried out to gain an enhanced understanding of the influence of PMI on the process and the process results.

The numerical studies include the determination of undeformed chip parameters and a detailed description of the machine model. After presenting different coupling strategies of KSIM and SFEM, the result of a combined simulation will be described.

B. Denkena and F. Hollmann (Eds.): Process Machine Interactions, LNPE, pp. 81–100.
springerlink.com

4.2 Experimental Investigation of Process Machine Interactions in Grinding

Experimental setup

The surface-up grinding experiments were executed on a high performance grinding machine with high stiffness. Two series of tests were carried out. In the first series, a resin bonded CBN (cubic boron nitride) grinding wheel (B181) with a diameter of Ø 400 mm and a width of 12 mm was used. The second series of tests was aiming at higher loads of the machine system to achieve higher displacements, corresponding to stronger PMI. To achieve these higher loads, i. e. higher grinding forces, specific material removal rates higher than those of the first series were necessary. Therefore, another grinding wheel had to be used. This grinding wheel was an electro-plated CBN grinding wheel (B251) with a diameter of Ø 400 mm and a width of 24 mm. The workpiece material used for both series of tests was a heat-treated steel AISI 4140H (42CrMo4V, DIN EN 10132-3, 55 ± 2 HRC) with dimensions of 125 mm x 50 mm x 10 mm.

Common measurement techniques were applied using a dynamometer for measuring normal and tangential forces and non-contact hall effect probe to measure the effective spindle power. In addition, the displacements of the grinding wheel relative to the headstock were measured (to examine the process machine interactions). The application of optical measurement systems was not possible due to the high amount of cooling lubricant, which was used during the experiments. Also, tactile sensors could not be used because of the high rotational speeds. For this reason, the displacements were measured using eddy-current sensors. They provide high-resolution signals and can be used in wet environments. In the first series of tests using the resin bonded grinding wheel, the measuring surface used for the sensors was a high-precision shoulder on the grinding wheel. In the second series of tests using the electroplated grinding wheel, the flange of the grinding wheel was used as measuring surface.

First series of tests – resin-bonded grinding wheel

The parameters used in the first series of tests are listed in Tab. 4.1. The focus of the experiments was the examination of PMI based on the measured displacements of the grinding wheel. Therefore, the influence of grinding wheel speed, feed rate and depth of cut was evaluated.

The average values of the normal grinding forces during stationary grinding ranged from $F_n = 300 - 1{,}100$ N, the tangential grinding forces ranged from $F_t = 50 - 300$ N. The displacements in normal and tangential direction reached 7 and 1 µm respectively. However, the displacements in tangential direction could not be reliably measured because of the small absolute values.

Table 4.1 Grinding parameters for first series of tests

grinding wheel	diameter 400 mm; resin-bonded; B181 V240 (DIN ISO 6106)	
grinding parameters	grinding wheel speed:	60 - 100 m/s
	depth of cut:	0.25 - 1 mm
	feed rate:	600 – 4,800 mm/min
	maximum specific material removal rate:	20 mm³/mm s
lubricant	cooling 300 l/min at 12 bar; wheel cleaning 100 l/min at 25 bar	

The relative dynamic stiffness during the stationary grinding process can be calculated based on the measured normal grinding forces and displacements . The calculated relative dynamic stiffness varies from 120 - 200 N/mm (Fig. 4.1). Variations of the wheel speed and the depth of cut do not influence the relative dynamic stiffness. The main influence on the relative dynamic stiffness in normal direction was exerted by the feed rate. Different feed rates result in different machine loading times. Feed rates of 1,200 mm/min or less reveal a relative dynamic stiffness of 120 - 160 N/µm. Feed rates of 2,400 mm/min or higher (grinding pass < 3 s) reveal an almost constant relative dynamic stiffness of approximately 200 N/µm. It seems that the inertia of the traveling column of the grinding machine of more than 10 tons influences the measured displacements due to the short time periods of loading.

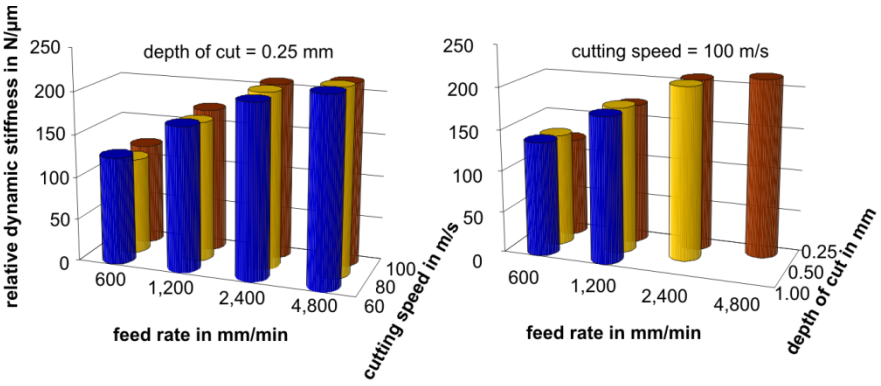

Fig. 4.1 Relative dynamic stiffness from the first series of tests

Second series of tests – electro-plated grinding wheel

As mentioned above, the electro-plated bonding of the grinding wheel used for the second series of tests allows much higher loads than the resin bonding. The maximum specific material removal rate investigated was 87.5 mm³/mms (Tab. 4.2).

Table 4.2 Grinding parameters for second series of tests

grinding wheel	diameter 400 mm; electro-plated; B251; 0.2 carat/cm²	
grinding parameters	grinding wheel speed:	63 - 100 m/s
	depth of cut:	0.25 - 2 mm
	feed rate:	1,000 – 6,000 mm/min
	maximum specific material removal rate:	87.5 mm³/mms
lubricant	cooling 420 l/min at 12 bar; wheel cleaning 110 l/min at 25 bar	

Compared to the investigations with the resin bonded grinding wheel the specific material removal rate was significantly increased. However, the measured normal and tangential grinding forces were smaller than the forces reached with the resin-bonding wheel (F_n = 140 - 780 N and F_t = 30 - 260 N). The resulting maximum measured displacements in normal direction were smaller (4 µm), too.

Similar to the first series of tests, the relative dynamic stiffness during the stationary grinding process was calculated based on the measured normal grinding forces and displacements. The relative dynamic stiffness ranged between 110 N/µm and 210 N/µm (see Fig. 4.2). The same correlations for the relative dynamic stiffness as for the resin-bonded grinding wheel were observed. Variations of wheel speed and depth of cut showed minor influence whereas the feed rate had a strong influence.

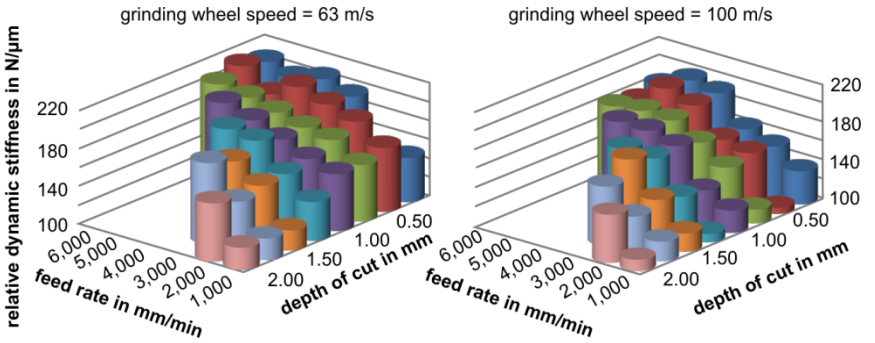

Fig. 4.2 Relative dynamic stiffness from the second series of tests

In this second series of tests, the quality of the ground workpieces was evaluated. The surfaces were classified into three categories:

- no grinding marks
- grinding marks
- grinding marks and burn

According to these categories, the whole parameter range can be mapped into acceptable process results (no grinding marks) and inacceptable process results

(grinding marks or grinding marks and burn). The classification of the ground surface was carried out visually since measurement with tactile sensors was not suitable. Fig. 4.3 shows the results of the mapped parameters.

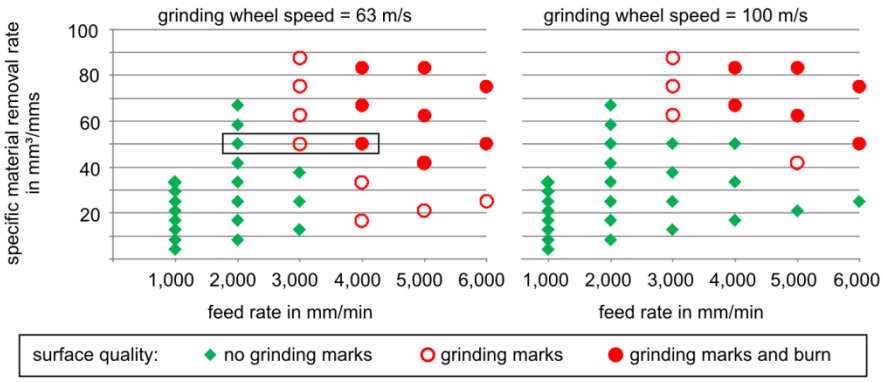

Fig. 4.3 Quality of the ground surface

Similar to the relative dynamic stiffness, the feed rate is the dominating factor for the occurrence of grinding marks and burn. This can be seen when comparing different feed rates at constant material removal rates (e. g. 50 mm³/mms at 63 m/s): At a feed rate of 2,000 mm/min there are no grinding marks or burn. However, at 3,000 mm/min grinding marks occurred. At 4,000 mm/min (and 6000 mm/min) grinding marks as well as burn were detected. The occurrence of grinding marks can be attributed to the higher feeding path per wheel revolution at higher feed rates and the resulting higher chip thicknesses. The observed burn was caused by less cooling lubricant volumes per time unit when applying higher feed rates. Less grinding marks and burn occurred at higher wheel speeds. This results from the better cooling lubricant supply at higher wheel speeds and to the smaller feeding path per wheel revolution.

Despite the correlation of the influence of feed rate on the relative dynamic stiffness and on the workpiece quality no direct correlation between these two parameters could be found. Higher relative dynamic stiffness does not necessarily result in higher or lower workpiece quality. When taking, for example, the feed rate 5,000 mm/min at grinding wheel speed 100 m/s the relative dynamic stiffness is approximately constant for all applied depths of cut. In contrast, the workpiece quality ranges from no grinding marks to grinding marks and burn.

4.3 Modeling and Simulation

4.3.1 Process Model

In the following, the process model used is presented. Therefore, the concept of the model is described and some simulation results are shown.

The process model used is based on a kinematic-geometrical simulation (KSIM) of surface and cylindrical grinding developed by Warnecke and Zitt [4, 5] and enhanced in further works [6, 7, 8]. The concept of the KSIM is based on the observed micro and macroscopic cause-and-effect chain in grinding. KSIM was developed and programmed in Fortran language as an offline tool for analyzing, dimensioning and optimizing grinding processes. In contrast to empirical process models, which correlate process inputs and process outputs mathematically, the KSIM simulates the grinding process as a penetration between the enveloping profile of the grinding wheel and the workpiece. Therefore, the micro and macro-geometry of the grinding wheel and the workpiece as well as the process kinematics have to be modeled.

To gain realistic simulation results the grinding wheel topography has to be modeled precisely. For this reason (in addition to the reproduction of the macro geometry), there is a special focus on the micro geometry of the grinding wheel. To model the topography in KSIM a "synthetic" generation of the grinding wheel was chosen instead of digitalizing the topography. This has the advantage that the modeling of the topography is not limited to the quality of the measuring system and to the available grinding wheels. Instead, the topography is generated based on microscopically-identified characteristic values.

The modeling of the micro-geometry in KSIM accounts for the stochastically-affected nature of grinding wheels. The geometrically-undefined shape as well as the unspecified number and distribution of the single abrasive grains are considered in KSIM. In modern high-performance, grinding tools are used, which consist of a metal body and diamond or cubic boron nitride (CBN) abrasive grains for the most part. Those tools use metallic, ceramic or resin bonding. Most modeling concepts of diamond or CBN grains use abstract descriptions via simple geometrical bodies [1]. With this method, the morphology of real grains is only roughly approximated. The modeling of the grains in KSIM is based on complex basic geometries (ellipsoid, tetrahedron, cuboid and octahedron) according to the possible crystal morphologies of CBN and diamond. These basic geometry models are modified under statistic variations to gain more realistic grain models. Different grain sizes can be regarded by the statistic distribution of the long and short grain axis l_{Al} and l_{Ak}. This detailed geometrical mapping of the grinding wheel topology in KSIM also enabled wear and dressing to be taken into account.

The KSIM simulates the grinding process by overlapping the modeled grinding wheel and a geometrically-modeled workpiece. The overlapping between grinding wheel and workpiece is given by the process kinematic, which can be calculated from the motion of the machine axis by a coordinate transformation. This coordinate transformation enables even complex process kinematics to be simulated based on the process type and machine setup.

The output parameters of the simulation are the experimentally not measurable undeformed chip thickness (h_{cu}), chip length (l_{cu}), chip width (b_{cu}) and chip cross section (A_{cu}) of every single grain. In the simulation, ideal cutting is assumed, which means that ploughing of material does not occur and each grain removes the whole material volume encountered. The superposition of every single grain contact enables the examination of the resulting macro and micro-geometry of the workpiece. Based on the simulated chip parameters a specific grinding force can

be calculated depending on the process type and the workpiece material. The chip cross section and the specific grinding force are used to calculate the forces of each single grain based on a simplified approach of Kienzle. The Kienzle approach can be used to calculate cutting forces, e. g. for turning or milling processes. The simplified approach is based on a specific cutting force $k_{c,sim}$ (an experimentally-determined parameter), the undeformed chip thickness and the width of the undeformed chip. The total process force can then be calculated by cumulating the forces from each kinematic grain (i. e. each grain that removes material) (Fig. 4.4).

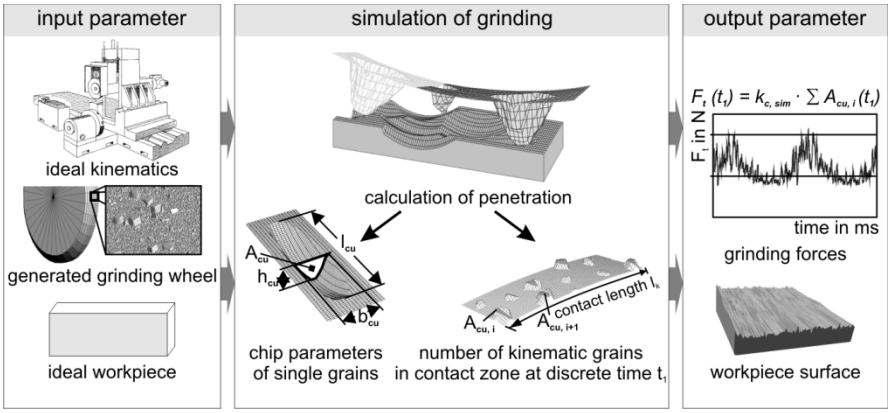

Fig. 4.4 Flow chart of the kinematic simulation

For the simulations to be carried out the modeled grinding wheel with the dimension of Ø 400 x 3 mm² was used. By using a smaller grinding wheel width than the wheel used in the experiments the calculation time of the kinematic simulation could be reduced (without reducing the simulation quality [9]).

Based on the applied manufacturing process (electroplating) a grain protrusion height of 35 % of the nominal grain size of 251 µm was used to model the grinding wheel. This means that about 163 µm of the grain height were embedded in the bonding, resulting in an average grain protrusion height of 88 µm. Because of the statistic nature of the modeling process the grain size distribution leads to significant deviations of the average grain protrusion height. This results in grains with high protrusion heights that remove the whole material, resulting in chip thicknesses of 10 to 15 µm. Those grains would wear very fast under real grinding conditions. This rapid wear would lead to a stationary grinding process characterized by a high number of kinematic grains distributing the material removal process over many grains with less chip thickness. Since in KSIM only one wheel revolution is simulated with no wear a numerical dressing process was implemented in KSIM to model grinding wheels in a stationary wear state [8]. Within this numerical dressing process, the grain protrusion height of every single grain is ideally cut down to a specified limit (dressing height, see Fig. 4.5) to fit real grinding conditions, for the simulations in this study 90 µm.

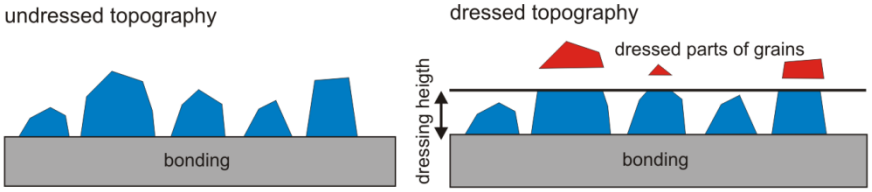

Fig. 4.5 Numerical dressing process

The simulated process parameters were chosen corresponding to those of the experimental investigations, which have been carried out. These parameters are listed in Tab. 4.3.

Table 4.3 Model specifications and process parameter for kinematic simulation

modeled grinding wheel	diameter 400 mm; width 3 mm; B251; 1,200 grains/cm²	
process parameter for kinematic simulation	grinding wheel speed:	63 - 100 m/s
	depth of cut:	0.5 - 1 mm
	feed rate:	1,000 – 5,000 mm/min
	maximum specific material removal rate:	83.33 mm³/mms

In each kinematic simulation, two grinding wheel revolutions are simulated. The first grinding wheel revolution is simulated with an ideally even workpiece. After this revolution, the contact zone is prepared, i. e. a ground surface is generated. The second grinding wheel revolution is then operated in this ground surface. This is comparable to a real grinding process where the grains always penetrate a ground surface in the contact zone. The following simulation results have been obtained from the second revolution (Fig. 4.6):

- mean value of the average chip thickness of all kinematic grains ($h_{cu,med}$) and
- number of momentarily active grains within the contact zone (N'_{mom}).

Generally, an increase of either the feed rate or the depth of cut results in higher specific material removal rates. This means that a higher material volume has to be ground in the same time, resulting in a higher chip thickness and a higher number of momentarily active grains. The results show a progressive increase for the chip thickness and a degressive increase of the number of active grains with increasing feed rate. The increase of active grains is limited due to the constant contact length at a constant depth of cut, which limits the maximum number of available grains for the material removal process. For this reason, the chip thickness shows a progressive increase because it has to compensate the degressive increase of active grains with increasing material removal rates.

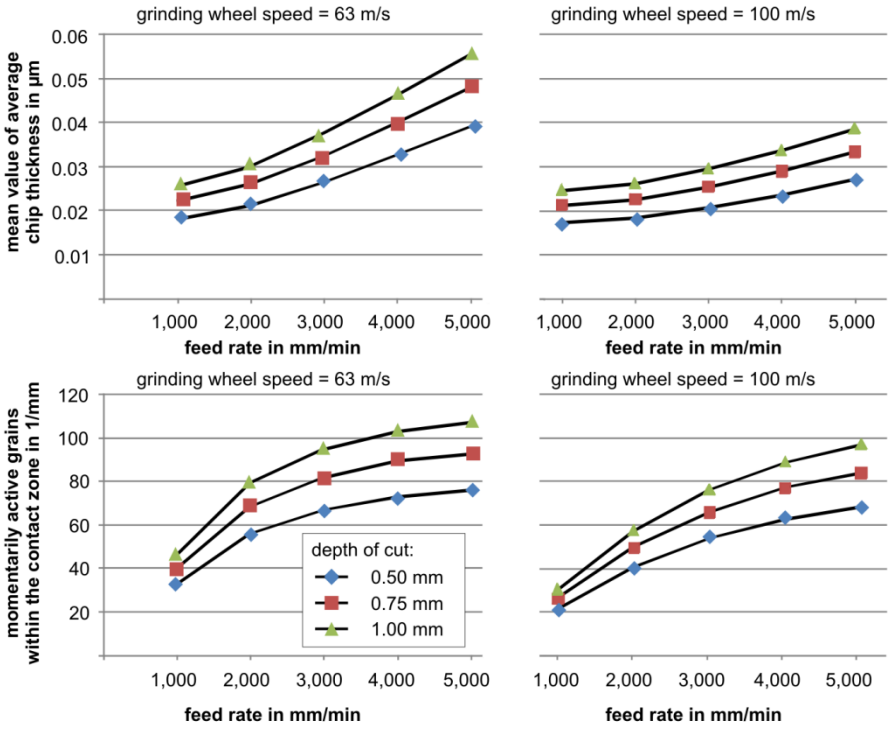

Fig. 4.6 Simulation results

A comparison of the average chip thickness and the number of active grains for different grinding wheel speeds reveals higher values for lower grinding wheel speeds. At higher grinding wheel speeds, less material has to be removed within each grinding wheel revolution. Thus, the chip thickness and the number of active grains decrease.

4.3.2 Machine Model

The modeling of the machine has been carried out by means of the finite element method on the base of the so-called Arbitrary Lagrangian Eulerian (ALE) approach. The system to be modelled consists of a grinding wheel, which rotates with a constant angular velocity (Fig. 4.7). The notations used are briefly explained in the following.

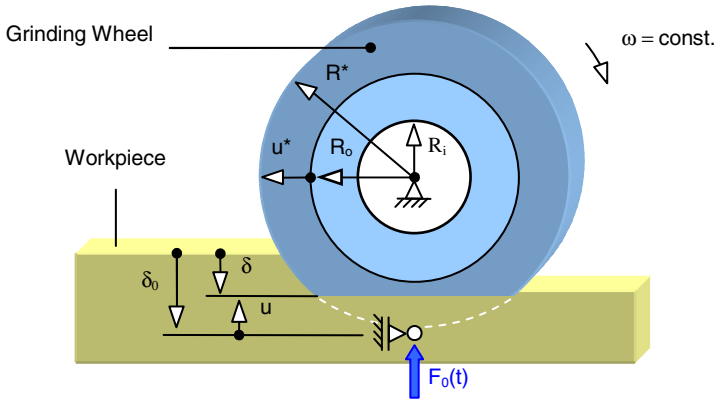

Fig. 4.7 Model of the grinding wheel. For the machine model there are two important radiuses: the inner radius R_i which the wheel is fixed at, and the expanded radius R* that serves as reference to determine the wheel's deformation

The grinding wheel has an inner radius R_i, which is assumed to remain constant throughout the simulation since the grinding wheel is fixed to the spindle. Due to the centrifugal forces caused by the angular velocity ω the outer radius R_o expands to the radius R* by the radial expansion u*.

Starting-up processes enabling the grinding wheel to accelerate from the idle state up to the velocity ω do not have to be considered. It will be assumed that at the time $t = 0$ the grinding wheel already rotates with the velocity ω and thus has the outer radius R*. The depth of cut, which the grinding wheel is initially plunging into the workpiece with, is denoted by δ_0. The cutting force resulting from δ_0 is denoted by F_0. Due to this force, which is assumed to only radially act at one point of the wheel's circumference, the grinding wheel deforms in radial direction by the amount u, defined relatively to the expanded radius R*. In tangential direction, the force application point is retained by defining an additional bearing. The deformation u is taken to be positive, if the outer radius R* increases. The depth of cut, which results when the machine's deformation is taken into account, is simply given by $\delta = \delta_0 + u$. According to this nomenclature one can distinguish initial values (δ_0 and $F_0(\delta_0)$), which are set up at the beginning of the process, and effective values (δ and $F(\delta)$), which result during the cutting process, for both the depth of cut and the cutting force.

The machine model can now be used either independently or in conjunction with a process model to run both uncoupled and coupled simulations respectively. Simulation results are presented in a later section.

4.3.3 Coupling Strategies

The basic concept of the coupling strategies is an exchange of the simulation results between the machine (SFEM) and process (KSIM) model. That means that the output data of one model is used as input data for the other model and vice

versa. The coupling algorithm is based on general modeling strategies for coupled problems, i. e. Neumann and Dirichlet boundary conditions are applied. In the following, four coupling strategies are presented. Strategies 2 and 4 are closely related to each other.

Coupling Strategy 1 - data exchange and iteration until convergence after multiple time steps (each wheel revolution)

The process model (KSIM), as presented in chapter 4.3.1, provides simulation results after every grinding wheel revolution. For this reason, data exchange of process and machine model is carried out after each grinding wheel revolution. The resolution of the simulated grinding force signal depends on the grinding wheel speed and the wheel diameter. Also, one grinding wheel revolution consists of a number of time steps (here 1,000), comparable to the number of data points for one revolution in real measurements. When modeling, for example, the grinding wheel presented in 4.3.1 (Ø 400 mm, grinding wheel speed 100 m/s) the simulated grinding force signal for one wheel revolution has a resolution of 80 kHz.

The coupled simulation starts with the generation of a force signal by the process model. For this force signal an ideal grinding machine is assumed, i. e. no machine deformations are considered. This force signal is used as input data for the machine model. The machine model generates displacements of the grinding wheel for one wheel revolution based on the input force signal. After resetting the workpiece topography (to simulate the same grinding wheel revolution as before) the process model is restarted based on the generated displacements by the process model. In doing so, the penetration of the grinding wheel and the workpiece is modified, which results in a different grinding force signal. This altered force signal again serves as input for the machine model and so forth. This iteration is repeated until “convergence” occurs, i. e. the simulated force and / or displacement signals (average values) of two consecutive iteration steps show minor deviations (Fig. 4.8).

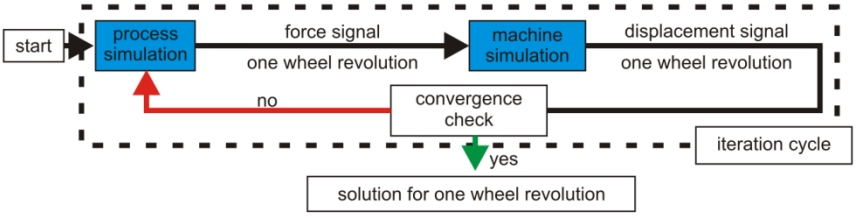

Fig. 4.8 Coupling strategy 1 - data exchange after each wheel revolution

Coupling Strategy 2 - data exchange and iteration until convergence for each time step

The principle of coupling strategy 2 is similar to that of coupling strategy 1. The difference is that the data exchange between the process and machine model (grinding force and displacement) is conducted after each time step within one grinding wheel revolution instead of the complete revolution (Fig. 4.9).

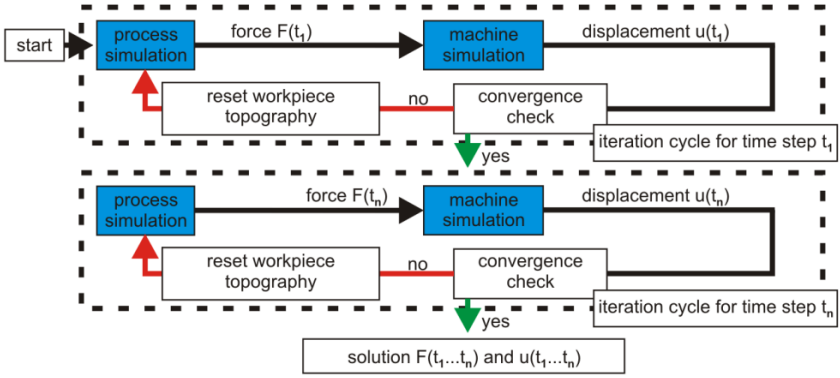

Fig. 4.9 Coupling strategy 2 - data exchange and convergence for each time step

In other words, coupling strategy 1 is applied for each single time step until convergence is reached. When convergence of force and / or displacement is achieved for the current time step the iteration cycle will be started again for the next time step. When using 1,000 time steps for one wheel revolution coupling strategy 2 consists of 1,000 iteration cycles, each with numerous iteration steps. This results in very large simulation times so that a simplification of each iteration cycle represents an interesting alternative solution, as will be discussed in coupling strategy 4.

The main advantage of coupling strategy 2 is the possibility to simulate only a part of one grinding wheel revolution. That means computing time can be saved, if less than one wheel revolution is needed.

Coupling Strategy 3 - asynchronous data exchange for each time step without iteration

In coupling strategy 3, no iteration cycles are used. As in coupling strategy 2, the force signal at time step t_n is used as an input for the machine model. The calculated displacement then serves as input for the process model, however, at time step t_{n+1} (Fig. 4.10).

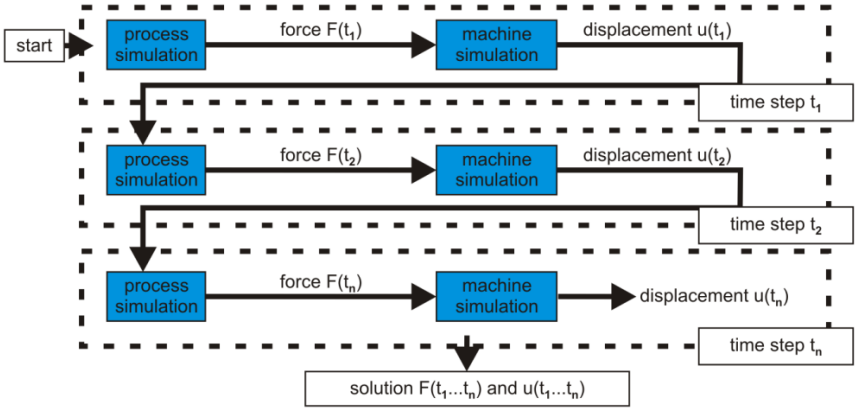

Fig. 4.10 Coupling strategy 3 - asynchronous data exchange for each time step

Coupling Strategy 4 - data exchange and iteration until convergence for each time step based on an empirical cutting force model

As already mentioned, this coupling strategy corresponds to coupling strategy 2 and represents coupling in a strong form. That means that a converged coupled solution is achieved at every time step. The coupling iterations are, however, carried out based on the assumption that the process force depends linearly on the cutting depth, i. e.

$$F_0(\delta_0) = c \cdot \delta_0 \tag{4.1}$$

where c denotes the "process stiffness". This assumption has been undertaken based on the linear relation between the chip cross section and the specific grinding force, to be found in the Kienzle approach, for example, and furthermore enables a considerable acceleration of the coupled simulation.

Eq. (4.1) is only valid for an ideally stiff grinding wheel, which the cutting depth is constant for throughout the whole process. For a real deformable grinding wheel, however, the grinding force is not a function of the cutting depth set up but of the actual (or effective) one. It will be assumed that the initial depth of cut δ_0 leads to a wheel deformation u, which simply has to be added to δ_0. By multiplying the sum $[\delta_0 + u]$ by the process stiffness c an adjusted force value is then obtained and can be subsequently used to calculate the deformation again. This coupling procedure can be written as:

$(\delta_0 \Rightarrow F_0 \Rightarrow u_0)$	$\Rightarrow$	$(\delta_1 \Rightarrow F_1 \Rightarrow u_1)$	$\Rightarrow \ldots \Rightarrow$	$(\delta_{conv.} \Rightarrow F_{conv.} \Rightarrow u_{conv.})$
uncoupled solution		1. coupling iteration		convergence iteration (coupled solution)

In summary, the models of the process, the machine and the process machine interactions presented above constitute a complete simulation procedure, which can now be used to run coupled simulations.

4.3.4 Coupling Results

The simulation results are summarized in Figs. 4.11 to 4.13. Of high interest for the following discussion are differences between the coupled and the non-coupled simulation.

A typical force signal generated by KSIM for one wheel revolution is given in Fig. 4.11a. A fast Fourier transform of the force signal shows a dominating contribution of frequencies of up to 5 kHz (Fig. 4.11b). Beyond this frequency, the grinding grits excite the machine at almost all frequencies.

The KSIM and SFEM models were coupled using coupling strategy 1. In SFEM, only static terms were activated just in order to check the convergence behavior of the coupled process machine system. Fig. 4.11c shows how the mean values over one grinding wheel revolution for the force and the displacement converge after about 6 iterations to 910 N and 6.2 µm respectively. These values are

smaller than the values gained after the first iteration (1,050 N and 7.2 µm), i. e. smaller than the values corresponding to the uncoupled solution.

Coupling strategy 1 is well suited for the case of quasi-static loading. In simulating a high-performance grinding process it has been observed that the high loading and deformation rates lead to an abrupt change of the state of single grits from contact to non-contact. This effect led to excessive fluctuations in the simulated force and deformation values causing the coupled simulation to diverge (despite the reasonable average values). For this reason, coupling strategy 1 is not suitable for coupled simulations involving vigorous dynamics.

In order to investigate dynamic properties of the coupled process machine system a coupling strategy, which guarantees a strong coupling has to be used, i. e. either strategy 2 or 4. The first one comprises more modeling details, the last is more economic in terms of simulation times. In addition, the fast Fourier transform of the force signal simulated in KSIM suggests carrying out the coupled simulation within a wide range of loading frequencies. In the following, the force signal provided by KSIM is substituted by a set of harmonic depths of cut with different frequencies ranging from 0 to 20 kHz. This set results in a set of harmonic loads, which are now able to excite the grinding wheel at different frequencies. The process machine interaction is then simulated using coupling strategy 4. The corresponding simulation model is based on the parameters listed in Tab. 4.4. All of them represent parameters commonly encountered in real grinding processes. For the process stiffness c a high value is used in order to emphasize the effect of coupling.

Table 4.4 Parameters for the coupled simulation, grouped into machine, process and coupling parameters

Machine model:		
Inner radius R_i	:	63.5 mm
Outer radius R_o	:	200 mm
Elastic modulus E	:	210 GPa
Poisson ratio ν	:	0.3
Material density ρ	:	7.85 g/ccm
Boundary conditions	:	– No displacement at the inner boundary. – No tangential displacement at the point the load is acting on.
Initial (setup) load $F_0(t)$	:	Results readily form the product $[c \cdot \delta_0(t)]$.
Process model:		
Angular velocity ω	:	200 rad/s, i. e. roughly about 2,000 rpm.
Depth of cut $\delta_0(t)$	:	Harmonic function with a fixed mean value of 5 µm, a fixed amplitude of 1 µm and variable frequencies ranging from 0 to 20 kHz.
Coupling model:		
Process stiffness c	:	200 N/µm

The time-dependent force and deformation signals are exploited in the following by means of their frequency and amplitude. Since the amplitude of a time dependent signal is generally not constant with respect to time the amplitude mean value over the whole signal is used.

The frequency spectrum of the grinding wheel can be obtained by varying the excitation frequencies and simulating the resulting mean deformation amplitude for each frequency. Also, the amplitude spectrum can be normalized by the deformation amplitude, which results when the grinding wheel is loaded by a quasi-static force. A normalized representation enables different simulation models to be compared to each other.

Fig. 4.12a shows how coupling shifts the eigenfrequencies gained from an uncoupled simulation to higher values. Note that the frequency spectrum obtained from a coupled simulation can no longer be considered as a property of the grinding wheel but of the whole system consisting of grinding wheel, process and interaction.

To answer the question as to why the eigenfrequencies increase when coupling is included one considers the applied force and the resulting deformation in time domain, Fig. 4.12b,c. All forces shown are normalized by dividing them by the same value, namely by the amplitude of the initial load $F_0(t)$, so that the initial and the effective force can be readily compared to each other with regard to both amplitude and frequency. However, all deformations are normalized by dividing them by their maximum value within the considered time interval. This has the advantage that, in normalized form, forces and deformations can be represented in the same diagram. A comparison of the frequencies is also possible. However, the deformation amplitudes resulting from different simulations cannot be readily compared to each other since deformations are not normalized by the same entity. Also, only some special loading frequencies will be presented here:

- the loading frequency of $f_0 = 12.8$ kHz, which corresponds to an eigenfrequency of the *uncoupled* process machine system and
- the loading frequency of $f_0 = 13.3$ kHz, which corresponds to an eigenfrequency of the *coupled* process machine system.

$f_0 = 12.8$ kHz

Although this loading frequency corresponds to an eigenfrequency of the grinding wheel as given in Fig. 4.12a there is no significant increase of the deformation amplitude throughout the coupled simulation. Fig. 4.12d shows that through coupling the effective force signal acquires smaller amplitudes than the initial one because a deformed grinding wheel generates a smaller depth of cut than an undeformed one. In the first excitation cycle, the maximum amplitude of the force effectively acting at the grinding wheel is only about 18 % of the initial force. Another more important aspect is the fact that through coupling the force signal acquires a higher frequency. This is the reason why the shifting effect observed in Fig. 4.12a occurs in direction of higher and not smaller frequencies. Fig. 4.12b shows that the force, which is effectively applied, and the resulting deformation oscillate with different frequencies. Under this circumstance, the deformation amplitude remained almost constant over the whole loading history. So, for resonance, effective force and deformation must first synchronize. This happens at the frequency of 13.3 kHz.

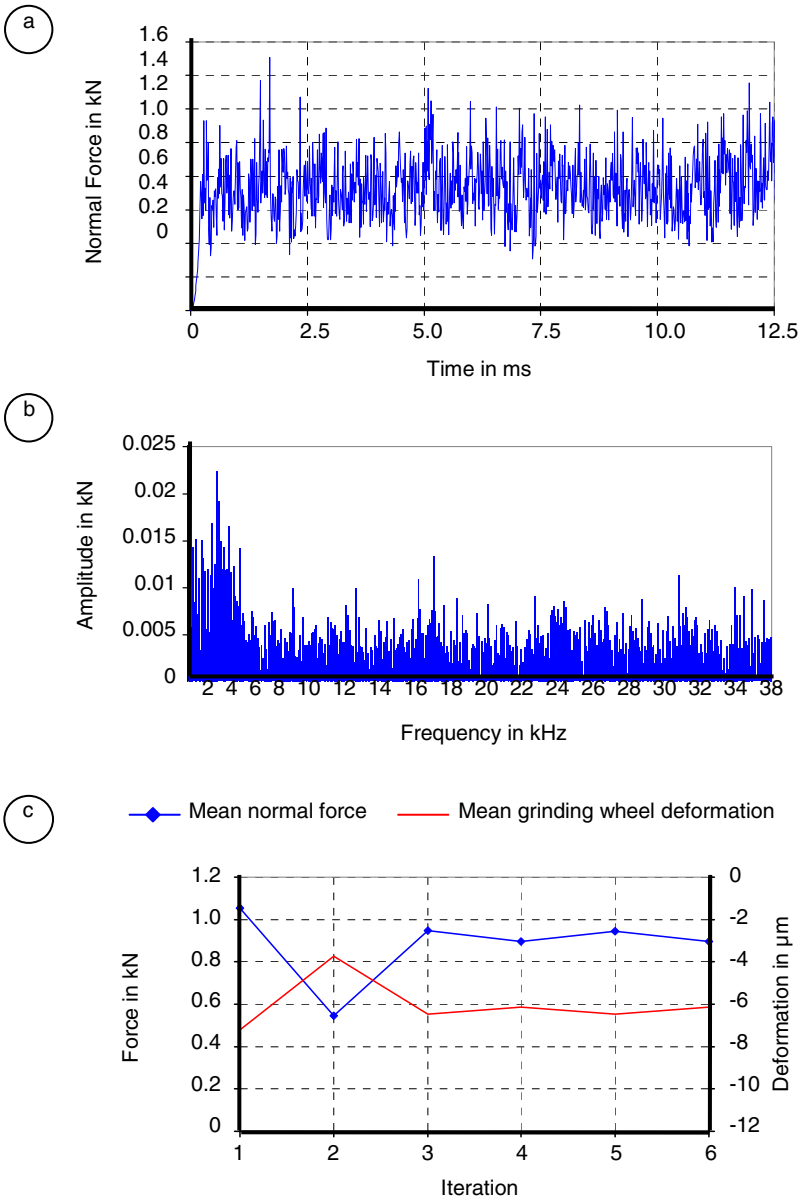

Fig. 4.11 Results of the coupled simulation based on coupling strategy 1. (a) Force signal simulated by KSIM. (b) FFT-transform of the force signal. (c) Convergence behavior of the coupled simulation.

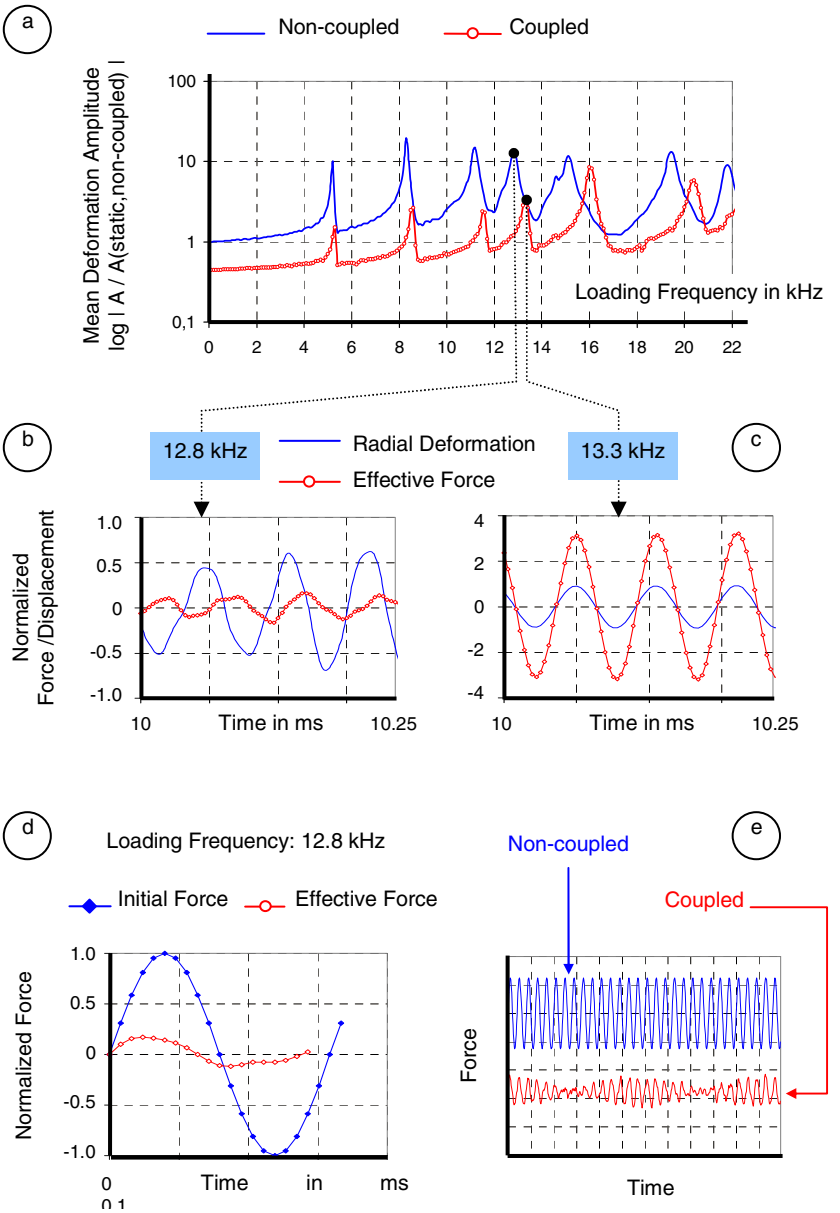

Fig. 4.12 Results of the coupled simulation based on coupling strategy 4. (a) Frequency spectrum. (b)-(c) Effective force and displacement in time domain for special loading frequencies. (d) Influence of coupling on the loading frequency. (e) Influence of coupling on the variation of the effective force over time.

f_0 = 13.3 kHz

As shown in Fig. 4.12c, effective force and resulting deformation oscillate for this loading frequency (after some loading cycles) with the same frequency. Only through their synchronisation can the coupled process machine system get into resonance.

Another important difference between the coupled and uncoupled system is that force and deformation are inversely influenced by each other. In the case of coupling, the deformation patterns resulting from a harmonic load, a beat for example, is mirrored into the force pattern and can thus also be retrieved there (Fig. 4.12e). This is not the case for an uncoupled simulation.

In Fig. 4.13, the eigenmodes of the grinding wheel are presented. They are just briefly described in the following. At the first eigenfrequency, the grinding wheel is oscillating in vertical direction and thus behaves approximately like a rigid body. The second eigenform represents an alternating dilation and contraction in horizontal and vertical directions. In the third eigenmode, the grinding wheel takes a triangular form. In the forth one, the outer wheel boundary expands and contracts uniformly. Finally, polygonal wheel forms result at higher eigenfrequencies.

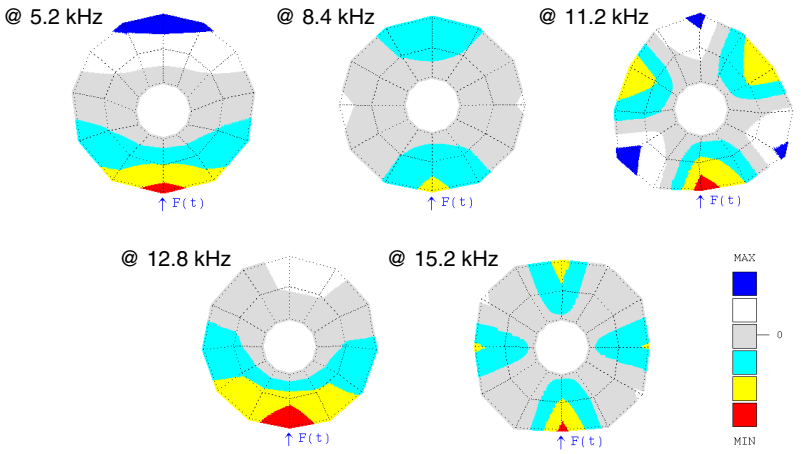

Fig. 4.13 Eigenmodes of the spinning grinding wheel (ω = 200 rad/s). The contour plots represent the field of the radial deformation. Positive values mean an increase in the extended radius of the outer wheel R* due to deformation.

4.4 Conclusion

Extensive experimental research was conducted to examine PMI during grinding. In doing so, displacements of the grinding wheel were measured and the resulting relative dynamic stiffness was mapped for a large parameter field. High stiffness was identified for high feed rates for different grinding wheels. The examination of the workpiece quality revealed grinding marks and burn when applying high

feed rates. The experiments conducted enhance the understanding of the cause-and-effect chain in grinding and the influence of PMI on the process and the process result.

Also, a complete simulation procedure enabling the modelling of the process, the machine and their interaction was discussed in detail. There are differences between results gained from uncoupled and coupled simulations, which can be summarized as follows:

In the uncoupled process machine system:

- Loading frequencies, which correspond to eigenfrequencies of the machine, lead to a critical (non-stable) process.
- The grinding force results in a machine deformation that, however, has no inverse influence.
- The knowledge of the frequency spectrum of the machine provides information about critical loading frequencies, which are not allowed, if the process has to be kept stable.

In contrast, simulations of the coupled process machine system revealed that:

- Coupling is more complex than just scaling the amplitude and the frequency of the initial load.
- A loading frequency, which corresponds to an eigenfrequency of the machine, does not necessarily lead to a critical process.
- Vice versa, a loading frequency, which lies outside the eigenfrequencies, can be critical.

The last three aspects suggest that the knowledge of the natural frequencies of the machine does not generally suffice to judge, whether a harmonic load is critical or not. This again underlines the importance of simulation techniques in general and of coupled simulations in particular.

Concerning simulation techniques one can say that there are quite efficient simulation techniques to simulate the deformation behavior of the grinding wheel due to transient process forces. This is primarily enabled by the use of the ALE-approach instead of the conventional Lagrangian one so that the kinematically less relevant rigid body motion is a priori omitted. This also enables the application of the force at a fixed point without contact-searching steps.

There is still need to bring simulation and experimental techniques closer together. Providing confident information about the real workpiece surfaces is still not reliably possible. Also, real-time simulations of high-performance grinding processes are currently not available.

The physical phenomena taking place during PMI are quite complex and not always accessible for measuring setups so that efficient simulation techniques are of great importance to investigate the grinding process. Although the simulation techniques presented in this chapter do not completely fit experimental results they can still be considered as an important step in understanding the phenomena involved in the PMI.

References

[1] Brinksmeier, E., Aurich, J.C., Govekar, E., Heinzel, C., Hofmeister, H.-W., Klocke, F., Peters, J., Rentsch, R., Stephenson, D.J., Uhlmann, E., Weinert, K., Wittmann, M.: Advances in Modelling and Simulation of Grinding Processes. CIRP Annals - Manufacturing Technology 55(2), 667–696 (2006)

[2] Aurich, J.C., Biermann, D., Blum, H., Brecher, C., Carstensen, C., Denkena, B., Klocke, F., Kröger, M., Steinmann, P., Weinert, K.: Modelling and Simulation of Process - Machine Interaction in Grinding. Production Engineering 3(1), 111–120 (2008)

[3] Herzenstiel, P., Bouabid, A., Steinmann, P., Aurich, J.C: Experimental Investigation and Computational Simulation of Process-Machine Interactions during High-Performance Surface Grinding. In: Proceedings of 1st International Conference on Process-Machine Interaction, PZH Hannover, pp. 267–278 (2008)

[4] Warnecke, G., Zitt, U.: Kinematic Simulation for Analyzing and Predicting High-Performance Grinding Processes. CIRP Annals – Manufacturing Technology 47(1), 265–270 (1998)

[5] Zitt, U.: Modellierung und Simulation von Hochleistungsschleifprozessen. Dissertation, TU Kaiserslautern (1999)

[6] Braun, O.: Konzept zur Gestaltung und Anwendung definiert gesetzter Hochleistungsschleifscheiben. Dissertation, TU Kaiserslautern (2008)

[7] Aurich, J.C., Herzenstiel, P., Sudermann, H., Magg, T.: High-performance dry grinding using a grinding wheel with a defined grain pattern. CIRP Annals – Manufacturing Technology 57(1), 357–362 (2008)

[8] Herzenstiel, P., Aurich, J.C.: Numerical and Experimental Investigations of a Grinding Wheel with a Defined Grain Pattern. In: CIRP Conference on Modeling of Machining Operations, vol. 12, pp. 567–574 (2009)

[9] Aurich, J.C., Herzenstiel, P., Kirsch, B., Steffes, M.: Experimental and Numerical Studies of a Surface Grinding Process. In: Proceedings of the 2nd International Conference on Process Machine Interaction (PMI) Session G1 (2010)